Understanding the selective etching of electrodeposited ZnO nanorods

Benoit N. Illy[1*], Bridget Ingham[2, 3], Michael F. Toney[4], Iris Nandhakumar[5*] and Mary P. Ryan[1].

[1] Department of Materials and London Centre for Nanotechnology, Imperial College London, London SW7 2AZ, U.K.

[2] Callaghan Innovation, P.O. Box 31-310, Lower Hutt 5040, New Zealand

[3] The MacDiarmid Institute for Advanced Materials and Nanotechnology, Victoria University of Wellington, P.O. Box 600, Wellington 6140, New Zealand

[4] Stanford Synchrotron Radiation Lightsource, SLAC National Accelerator Laboratory, 2575 Sand Hill Road, Menlo Park, CA 94025

[5] School of Chemistry, University of Southampton, Southampton SO17 1BJ, U.K.

KEYWORDS Zinc Oxide, Electrodeposition, Tubes, Dissolution, In-situ XANES

ABSTRACT: ZnO nanotubes were prepared by selective dissolution of electrodeposited nanorods. The effect of solution pH, rod morphology and chloride ion concentration on the dissolution mechanism were studied. The selective etching was rationalized in terms of the surface energy of the different ZnO crystal faces and reactant diffusion. The nanorod diameter and chloride concentration are the most influential parameters on the dissolution mechanism because they control homogenous dissolution or selective etching of the (110) and (002) surfaces. Bulk solution pH only has an effect on the rate of dissolution. By accurate control of the dissolution process, the nanomorphology can be tailored and the formation of rods with a thin diameter (10-20 nm), cavity or *ultra*-thin-walled tubes (2-5 nm) can be achieved.

INTRODUCTION

The formation of zinc oxide (ZnO) nanostructures has attracted a large amount of interest due to their range of potential applications *e.g.* sensors[1], photovoltaic cells[2] and nanogenerators[3]. ZnO nanomaterials are one of the richest families in terms of structural variety. Numerous nanomorphologies have been created in recent years: rods[4], 'nanocombs'[5], plates[6], hierarchical nanostructures[7], discs[8] and nanotubes[9]. Whilst a large amount of work has focused on the study of 1D nanostructures *via* either self-organized or templated assembly, hollow structures have received relatively little attention. The production of tubular structures results in a higher surface-to-volume ratio than wires or rods and this can be a key advantage

for photovoltaic[10] and sensing applications[11]. The production of nanotubes has been achieved using physical vapour deposition[12], pulse laser deposition[13], chemical vapour deposition[14], radio frequency magnetron-sputtering[15], hydrothermal reaction[16], chemical bath deposition[9], template-based growth[17] and electrodeposition[18-27].

Electrodeposition is a low cost and environmentally friendly technique. It allows careful control of the nanostructure morphology through the deposition parameters and it is widely used in industrial processes. The electrodeposition of ZnO nanotubes has been reported by both a one step process[18-20] and a two step process.[21-29] The one step process does not allow fine control of the nanotube dimensions (e.g. length, diameter and wall thickness). As the properties of materials at the nanoscale are strongly dependent on surfaces and interfaces, a two step process to form hollow structures is generally considered to be preferable because it allows better tuning of the nanostructure morphology: the wall thickness and depth of the tube diameter and length can be controlled independently.[21-26] In the two step process, the first step is the electrodeposition of ZnO nanorods, followed by selective etching. The deposition process is now well-understood;[30] under an applied potential, dissolved oxygen and nitrate ions are reduced according to reactions [1] and [2] and produce hydroxide ions which increase the local pH in the vicinity of the substrate surface and lead to the direct formation of crystalline zinc oxide (reaction [3]). This precipitation reaction is a result of the pH dependence on the solubility of ZnO (over $Zn(OH)_2$ for example).[31]

[1] $NO_3^- + H_2O + 2e^- \rightarrow NO_2^- + 2OH^-$

[2a] $O_2 + H_2O + 4e^- \rightarrow 4OH^-$

[2b] $H_2O + O_2 + 2e^- \rightarrow HO_2^- + OH^-$

[3] $Zn^{2+} + 2OH^{-} \rightarrow ZnO + H_2O$

The second step consists of the selective etching of the ZnO nanorods. To understand this process, it is necessary to consider the ZnO crystal structure. In the ZnO wurtzite crystalline structure, the top (001) face of the crystal is polar whereas the sides (110) are neutral (see Figure 1). The polar faces are meta-stable and may be dissolved preferentially.[9] As ZnO is an amphoter it can dissolve according to either reaction [4a] or [4b] depending on the solution pH:

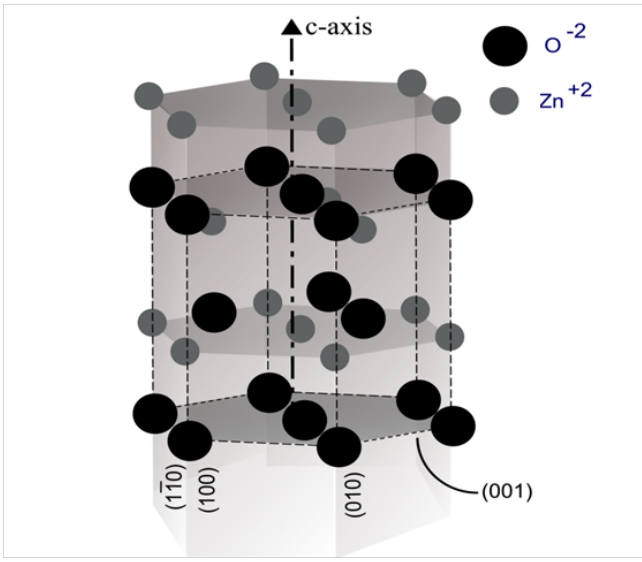

Figure 1. Schematic representation of the ZnO wurtzite structure.

The (001) plane is comprised of either O^{2-} or Zn^{2+} and is polar. The (110), (100) and (010) planes are comprised of an equal number of O^{2-} and Zn^{2+} and are thus electrically neutral.

$ZnO + H_3O^{+} \rightarrow Zn^{2+} + OH^{-} + H_2O$ [4a]

$ZnO + H_2O + 2OH^{-} \rightarrow Zn(OH)_4^{2-}$ [4b]

Such selective dissolution is however not always observed. For example Gan *et al.* report that rods with a diameter of 100 nm or smaller cannot be etched in an alkaline solution.[23] When selective dissolution

has been observed, two suggested mechanisms have been reported. The etching can happen either from the side[22, 23, 29] or the center[21, 26-28] of the top surface leading to the formation of tubes with a conical or rectangular tip respectively. It is currently not well-understood what controls the dissolution mechanism;[27] one of the main reasons is that the dissolution mechanism has only been studied by *ex-situ* characterization methods that gave poor insight into the kinetics of the process. The formation mechanism of nanostructured rods has been extensively studied by our group[6, 30, 32-38] and others and *in-situ* characterization techniques have been developed.[35-37] Together with *ex-situ* characterization these are powerful tools to relate changes of morphology with the experimental parameters and understand the dissolution process.

Several works have studied the effect of the dissolution conditions on the conversion of nanorods to nanotubes.[23,27,28] Elias *et al.*[27] have investigated the influence of Cl^- concentration and temperature on ZnO nanotube formation by *ex-situ* SEM characterization. They found that the dissolution of the nanorod core occurs for concentrations of $Cl^- \geq 1$ M and the dissolution rate increases with the temperature but these two parameters do not change the mechanism. The dissolution process has been studied in an alkaline potassium hydroxide aqueous solution by *ex-situ* SEM characterization with concentrations from 0.1 to 0.25 mol.L^{-1}.[23] It was found that the concentration of KOH has a strong effect on the dissolution rate and that a concentration of 0.25 mol.L^{-1} resulted in the degradation of the lateral walls but does not influence the mechanism. She *et al.*[28] report that the process of formation of nanotubes is similar in acidic (0.001 M HCl) and alkaline (0.125 M KOH) media.

The underlying factors governing the changes in mechanism are not known. In this paper the effects of pH, rod-morphology and chloride concentration are investigated and the different selective etching processes observed in aqueous solution are rationalized by correlating *in-situ* growth and dissolution measurements with *ex-situ* imaging and X-ray diffraction.

EXPERIMENTAL

ZnO nanostructures were cathodically deposited from $Zn(NO_3)_2$ solutions using a standard three electrode configuration. Au-coated glass slides were used as working electrodes onto which the ZnO nanostructures were deposited, with a platinum wire as a counter electrode and a potassium chloride saturated silver/silver chloride reference electrode. An ACM instrument Gill AC computer-controlled potentiostat was used. Prior to the electrodeposition the substrates were washed with acetone and deionized water. The electrolytic aqueous solution contained $Zn(NO_3)_2$ (Riedel DeHaën, 98%) and KCl (BDH, 99%) or $CaCl_2$ (BDH 90%) as the supporting electrolyte. Oxygen was bubbled through the cell for 20 minutes prior to deposition until the end of the experiment in order to ensure complete saturation of the solution. The temperature was 65 ± 2°C. The pH was adjusted through the addition of small quantities of HCl.

After 20 minutes the applied potential was switched off and the system monitored at open circuit potential for a further 5 minutes. The temperature during the dissolution was maintained at 65 ± 2°C.

In-situ x-ray absorption spectroscopy (XAS) experiments were used to monitor film growth and dissolution directly; full details of the experimental procedure have been given previously[35, 36]. The crystal structure was investigated by synchrotron X-ray diffraction (XRD) on beam line 11-3 of the Stanford Synchrotron Radiation Lightsource. The X-ray wavelength was 0.9736 Å. A point detector consisting of Soller slits with 2 milliradian resolution was used. Morphological characterization of the resultant nanostructures was carried out using a LEO GEMINI 1525 Field Emission Scanning Electron Microscope (FESEM), operating in-lens with an accelerating voltage of 5 kV. The film thicknesses were measured directly by FESEM from cross sections obtained by cleaving the films.

RESULTS

Figure 2 shows the increase in film thickness (actually measured as volume of ZnO per unit area) versus time for a sample grown at -770 mV Ag/AgCl, obtained from XAS measurements at fixed energy above the Zn edge (intensity at 9725 eV), using the approach described in references 35 and 36.

In Figure 2 the thickness increase during the deposition is apparent; a 2-stage growth process (regions I and II) occurs, which is characteristic of a transition from 3d to 1d growth in the nanostructured films[36]. The volume of material is then seen to slowly decrease at an effective rate of about 1nm per minute as soon as the cell is returned to open circuit conditions (region III). This is consistent with the formation of tubular structures by dissolution of ZnO. The inset (i) in Figure 2a shows a typical FESEM image of a dense film of nanorods removed from the electrolyte immediately at the end of deposition and inset (ii) the corresponding structure after 270 minutes dissolution at open circuit potential in the same solution.

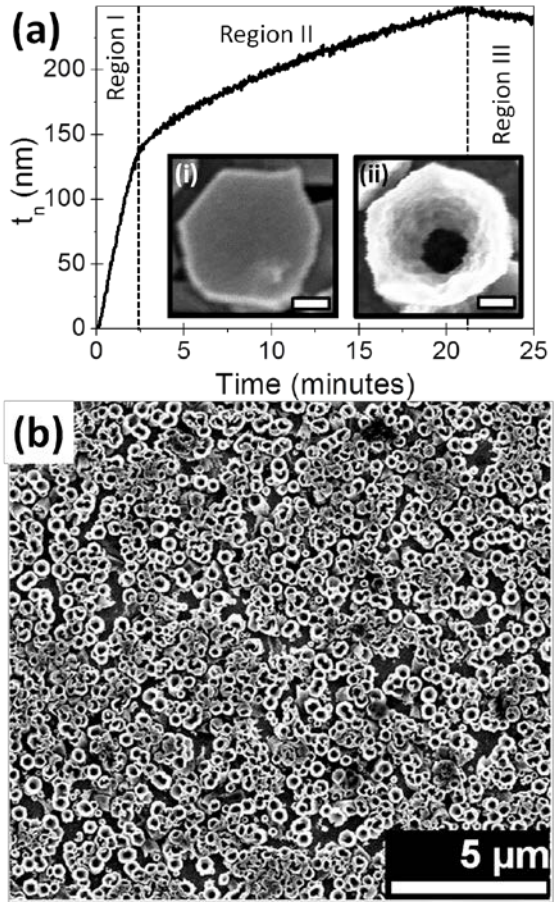

Figure 2. (a) Equivalent film thickness (volume per unit area assuming bulk density) obtained as a function of time, for a ZnO film deposited from 5 mM $Zn(NO_3)_2$ solution with 0.1 M $CaCl_2$ as the electrolyte at 65°C. The pH was 5.5. The applied potential was -770 mV Ag/AgCl. Region I corresponds to nucleation, II to 1d growth, and III to open-circuit dissolution. The inset micrographs correspond to the end of deposition (20 minutes, i) and dissolution (270 minutes, ii). The scale bar is 100 nm. (b) SEM micro-

graph obtained after 270 minutes dissolution, showing homogeneous formation of tube structures over large areas.

Before dissolution the film is composed of an array of coalesced nanorods oriented perpendicular to the substrate as a result of anisotropic growth along the c-axis, as is well-known in this system.[4] The rod length is about 350 nm normal to the substrate. The micrograph inset (ii), corresponding to the end of the process, shows the dramatic inhomogeneous nature of the dissolution process: holes are formed in the centre of the initial nanorods and preferential etching of the rod interior proceeds. This process is remarkably homogeneous over large areas (Figure 2b), for certain experimental conditions. The formation of nanotubes in this work has been observed for potentials ranging from -0.5 V to -1V and for Zn^{2+} concentrations from 5 mM to 10 mM. In order to gain a better understanding of the crystallographic effects, XRD measurements were performed. Figure 3 shows *ex-situ* grazing incidence scans of two films deposited from a 10 mM $Zn(NO_3)_2$ solution with 0.1 M KCl electrolyte at 65°C and an applied potential of -770 mV, one removed from solution immediately after 20 minutes deposition and the other subsequently dissolved at open circuit potential for 45 minutes.

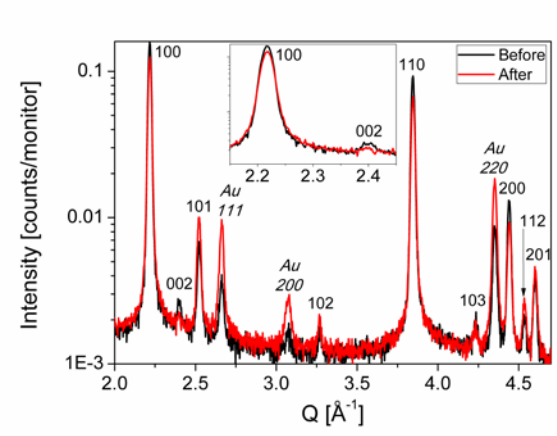

Figure 3. Grazing incidence x-ray diffraction scans of two films deposited for 20 minutes from a 10 mM $Zn(NO_3)_2$ solution with 0.1 M KCl electrolyte at 65°C and an applied potential of -770 mV Ag/AgCl, one removed from solution immediately after deposition but before dissolution (black), and the other subsequently dissolved for 45 minutes (red). The peaks are labelled according to the ZnO wurtzite struc-

ture or Au face-centered cubic (fcc) structure (italics). Note that the intensity is shown on a log scale. The inset shows a magnified view of the (100) and (002) peaks.

In the grazing-incidence geometry the incident X-ray beam is at a small angle (0.4°) to the sample surface. The penetration depth of the X-rays into the substrate is consequently low, and one measures diffraction from planes perpendicular to the sample surface. All the peaks have been identified as wurtzite ZnO or substrate Au and are labeled accordingly. An increase in the Au peak intensity is observed after dissolution due to the volume decrease of ZnO covering the substrate. The relative enhancement of the (100) and (110) peaks and the suppression of the (002) peaks relative to the isotropic powder reference pattern show that the nanostructures are oriented with the (002) direction predominately normal to the substrate.

In addition, radial and chi scans were performed on a selection of peaks: (100), (110), (101) and (002). The radial scans (at different chi) were each fitted to a Gaussian peak function to obtain the area, position and full width at half maximum. The specular (002) peak shows a reduction of the signal to 41% of the original intensity as a result of the dissolution. The (100) and (110) are in-plane, and thus, it is difficult to accurately quantify their intensities. The (101) has both in-plane and out-of-plane components and shows a reduction of 49%. Therefore the dissolution process over 45 minutes results in 40-50% of the ZnO material being dissolved, which is consistent with the XANES result obtained under the same conditions.

In the following parts, the effect of pH, rod-morphology and chloride concentration on the dissolution rate and mechanism are investigated.

Effect of pH

Table 1 shows the dissolution rates in Region III (Fig. 2) as a function of pH. At pH 3 a ZnO film is totally dissolved in a few minutes once the cathodic current is removed. At pH 4 and above, the dissolution rate is slow and good control over the nanotube dimensions can be achieved.

pH	Dissolution rate (nm/min) *
3	70.96 ± 0.37
4	3.20 ± 0.12
5	1.19 ± 0.14
6	1.22 ± 0.14

Table 1. Dissolution rates for ZnO nanostructures as a function of pH. *The rates are calculated from *in-situ* X-ray absorption measurements such as those shown in Figure 2.

No change in dissolution rate is observed within the uncertainties between pH 5 and pH 6. No morphological changes in dissolution behavior are observed when changing the solution pH from 4 to 6 by *ex-situ* FESEM and the structures are similar to the one presented in Figure 2. The selective dissolution occurs from the centre of the top surface to the bottom resulting in tubular structures in agreement with the results of She *et al.*[26] and Elias *et al*.[27] who suggest that the pH only affects the dissolution *rate* and not the mechanism. The electrodeposition of ZnO nanorods is well-studied and by tuning the deposition conditions such as the applied potential and zinc precursor concentration the length and diameter of the nanorods are readily controlled. For example, by increasing either the Zn^{2+} concentration in solution or the applied potential, the size of the rods can be increased[30]. Table 2 summarizes the deposition condi-

tions used in this study and the resulting dimensions and dissolution rates. The effect of the rod length, diameter and Cl^- concentration on the dissolution mechanism can thus be independently studied.

	E mV	$[Zn^{2+}]$ mM	$[Cl^-]$ M	t min	D nm	L nm	R nm/min
a	-770	1	0.1	60	44	594	0.66± 0.11
b	-370	5	0.1	20	43	181	0.64± 0.15
c	-670	5	0.1	20	103	175	0.79± 0.13
d	-770	5	0.1	20	125	239	1.19± 0.14
e	-770	10	0.1	20	197	381	3.30± 0.21
f	-770	5	0.2	20	203	398	1.22± 0.14
g	-870	5	0.2	20	250	490	-

Table 2 Experimental conditions, rod dimensions and dissolution rates for ZnO nanostructured films studied. t, D, L and R are the dissolution time, rod diameter, rod length and rate of dissolution respectively. *Rates are calculated from *in-situ* x-ray absorption measurements such as shown in Figure 2. The dissolution rate for experiment g was not measured. The solution pH was 5.5 ± 0.5 for all solutions.

The dissolution rate in Region III (Figure 2) is found to be independent of the rod dimensions for the smaller structures (experiments a and b in Table 2). Above 100 nm diameter the dissolution rate increases with the rod dimensions. *Ex-situ* SEM characterization realized after, and at selected time points during, the dissolution process show that the changes observed in dissolution *rates* are linked to striking changes in dissolution *behavior* (see Figures 4 and 5: note that labels in both figures correspond to conditions listed in Table 2).

For the smaller nanorods the dissolution is homogenous: both the diameter and the length are decreased and no selective etching is observed (see Figures 4a and 4b). When the dimension of the nanostructures is further increased (diameter >100 nm) a selective etching resulting in tube formation is observed (Figure 4 c and d, and Figure 5).The initiation of tube formation is seen in Figure 5 where a 'pit' is formed at the centre of the top surface of the nanorods (see Figure 4c). A similar dissolution behavior is observed when the diameter is increased further still: the dissolution rate is increased and the resultant wall thickness is decreased (see Figure 5g3). Occasionally tube wall-collapse was observed when they became very thin.

Changing the concentration of Cl^- from 0.1 to 0.2 M dramatically changes the dissolution kinetics as shown in Table 2. For rods with similar dimensions, the dissolution rate decreases dramatically from 3.30 to 1.22 $nm.min^{-1}$ respectively (see Table 2, e and f)

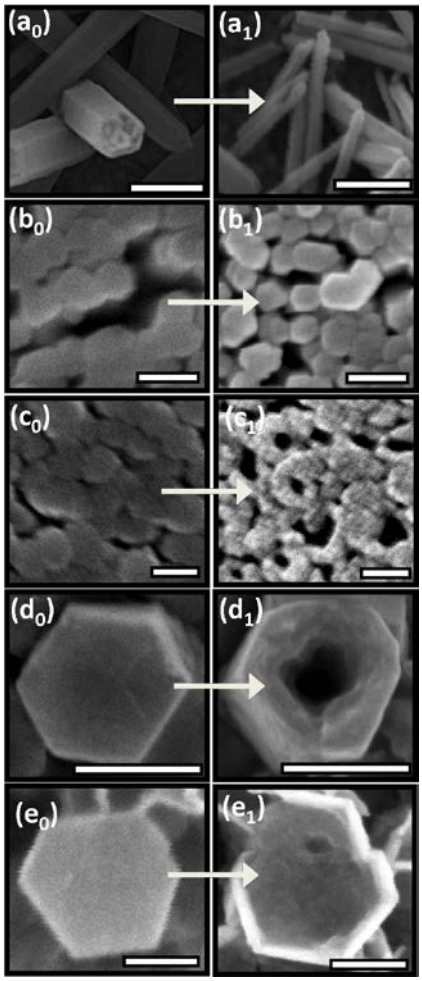

Figure 4. Study of the nanorod dissolution as a function of rod dimensions: FEG-SEM images of films before (a_0, b_0, c_0, d_0 and e_0) and during dissolution (a_1, b_1, c_1, d_1 and e_1). (a_0): D=44 nm, L=594 nm (a1) after 210 minutes dissolution, (b_0): D=43 nm, L=181 nm (b1) after 45 minutes dissolution, (c_0): D=103 nm, L=175 nm, (c1) after 45 minutes dissolution, (d_0): D=125 nm, L=239 nm, (d1) after 45 minutes dissolution and (e_0): D=197 nm, L=381 nm, (e1) after 45 minutes dissolution. D and L are the rod diameter and length respectively. (see Table 2 for experimental parameters corresponding to (a) through (e)). The scale bars are 100 nm. (note that a) and b) are not the same rods: each image shows a representative image of the structures at a given time; we note that the material behavior is remarkably homogenous over large areas and the individual nanostructures all follow the same dissolution pattern for a given set of conditions)

The FESEM images in Figure 5f and 5g show that the mechanism of dissolution has also changed. No dissolution is observed after 45 minutes (picture not shown). Figures 5f1 and 5g1 show the FESEM images after 60 minutes dissolution. Several pits are formed on the side of the top of the rods (as opposed to in the middle). For longer dissolution times (see Figures 5f2 and 5g2), pits are extended from the sides towards the core of the rods whereas the top (002) surface is mostly preserved (see Figures 5f2 and 5g2). Figures 5g2 shows the formation of a cavity inside the nanorod. For longer dissolution times the (002) top surface collapses and nanotubes are formed. A similar dissolution behavior has been reported by Yan *et al.*[29], and is consistent with TEM analysis by Elias *et al*[27]who showed dissolution only *via* the (002) surfaces and not the (001) faces.

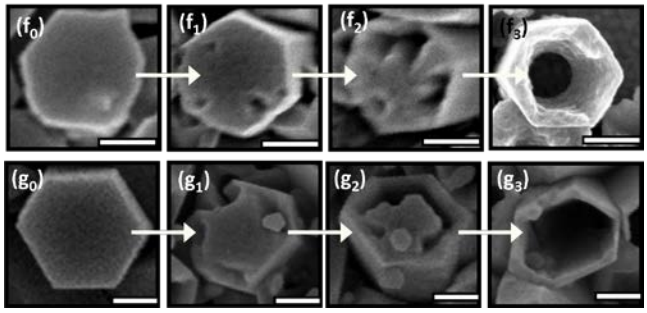

Figure 5. Study of the nanorod dissolution as a function of rod dimensions. FEG-SEM images of films before and during dissolution. 0 subscript images present the initial structures. Top: sample f, (f_0): D=203 nm, L=398 nm (f1), (f2) and (f3) after 60, 180, and 270 minutes dissolution respectively and, bottom: sample g, (g_0): D=250 nm, L=490 nm (g1), (g2) and (g3) after 60, 180, and 270 minutes dissolution respectively. D and L are the rod diameter and length respectively. (see Table 2 for experimental parameters corresponding to (f) and (g)).The scale bars are 100 nm.

DISCUSSION

Previously, the dissolution of electrodeposited ZnO nanorods has been mainly rationalized in terms of metastability of the (002) polar face: the metastability of the (002) plane leads to the preferential etching of the (002) plane and thus fastest etching rate in the [002] direction. However two important experimental observations remained misunderstood: why the dissolution of rods with a diameter lower than

100 nm does not lead to the formation of nanotubes and what is controlling the two dissolution behaviors experimentally observed (dissolution starting from the centre versus the corner of the top of the rods)? She and co-workers have proposed that the preferential etching at the centre of the nanorods was partly due to higher concentrations of defects in that region.[26] This hypothesis however cannot explain the homogenous dissolution or the formation of pits on the side of the top surface experimentally observed. To understand the selective etching the energy of all the faces and the reaction at the interfaces must be considered. Wander and Harrison calculated the surface energies of (100), (110) and (002) faces using an *ab initio* (all-electron) approach[39] and found this to be 2.32 $J.m^{-2}$, 4.1 $J.m^{-2}$ and 5.4 $J.m^{-2}$ respectively. The (002) has the highest surface energy which is only by a factor of 2.3 smaller compared to the most stable faces. Small electrochemical changes at the interface between the solution and ZnO may change the surface reactivity. We propose to explain the change in dissolution behavior from homogenous dissolution to preferential etching along the <002> direction observed when the rod diameter is increased from 40 nm to 100 nm by considering both the effect of the surface energies of the faces of individual rods as well as diffusion limitations on the dissolution reaction as a result of the nanoscale morphology (see Figure 6). The (002) planes are well-documented to be the most unstable; they have the highest energy[39] a fact that is normally exploited during the formation of nanowires and rods. Here this instability leads to preferential dissolution. Once dissolution starts the effect on the solution chemistry must be considered in order to understand the morphology evolution. Initial dissolution of the (002) surface leads to an increase in concentration of Zn^{2+} and OH^{-} ions at the vicinity of the top face according to reaction [4a]:

i) Rods with a small diameter (40 nm) lead to the formation of extremely small holes or channels at the top of the rod (< 40 nm). The diffusion of ions out of these channels is slow due to the small dimensions and so the Zn^{2+} and OH^{-} ions accumulate, changing the local chemistry and the dissolution rate at these sites is reduced. On the *outside* of these rods, even though the driving force of the dissolution is initially lower due to the lower surface energy, the diffusion of species away from the interface is faster and the

observed dissolution rate now becomes comparable with the top surfaces. As a result homogenous dissolution is observed *without* tubes being formed.

ii) For rods with a large diameter (100 nm), the top surface is larger and the incipient dissolution channels are wider allowing a rapid diffusion of the dissolution product away from the material and the formation of a tube. Here we expect some thinning of the edge of the tube through dissolution of the non-polar faces but the rates of dissolution of the two faces remain significantly different.

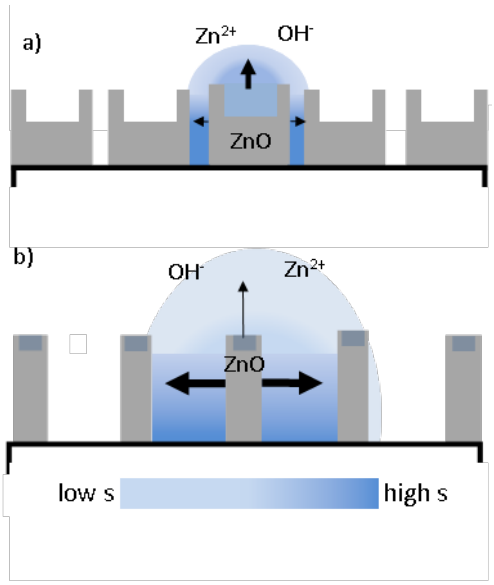

Figure 6. Schematic illustration of the change in dissolution behavior of ZnO when the rod diameter is increased. a) large diameter(>100 nm) and b) small diameter (<100 nm). The arrows represent the diffusion of the species produced by the dissolution of ZnO. The product of the reaction [4b] ($s=[Zn2+][OH^-]^2$) is indicated by the colour intensity. For rods with a large diameter (a), the dissolution behavior is governed by the surface stability and the top surface is dissolved preferentially. For rods with a smaller diameter (b), the dissolution of the top surface is limited by the low diffusion rate, and the dissolution is homogeneous.

Similarly the effect of Cl^- can be explained in terms of the change in surface energies: Cl^- ions are known to be absorbed on, and to stabilize the (002) polar surfaces reducing the surface energy of this face.[40] We note that the initial surface energy of the (110) vs (002) is 4.1 $J.m^{-2}$ vs. 5.4 $J.m^{-2}$; following

Cl^- absorption onto the (002) surface the surface energy of the (002) face is decreased (due to reduction of the charge density of this polar surface by the adsorbed species[41]) and the low index diagonal faces such as (110) become the least stable in the structure. Dissolution is now expected to occur preferentially along these directions and intermediate rates of dissolution are obtained.

The selective etching process gives one more condition by which the nanomaterials' morphology can be controlled. For rods with an initial diameter smaller than 100 nm, the formation of tubes is not observed and the nanorod diameter can be reduced after deposition (see Figure 4b). The wall size of the nanotubes can also be adjusted. It is possible to create ultra-thin tube walls by varying the deposition potential: Figure 7 shows tubes formed under the same conditions as in Figure 4e (dissolution) but for rods *formed* at a more negative potential. The wall thickness is decreased from ~50 nm to less than 20 nm and some walls are in the range 2-5 nm. At these dimensions one would expect to begin to observe quantum confinement effects. For example, it has been shown that quantum size confinement can significantly enlarge the exciton binding energy and band gap[42]. In addition the structures created have virtually no polar surfaces and so may exhibit distinctly different properties to other ZnO nanostructures.[33, 38] Moreover, the free surface area of these structures is at least 180% greater than the initial rods providing an easy way to enhance the performance of devices e.g. catalysts, gas sensors and solar cell applications.

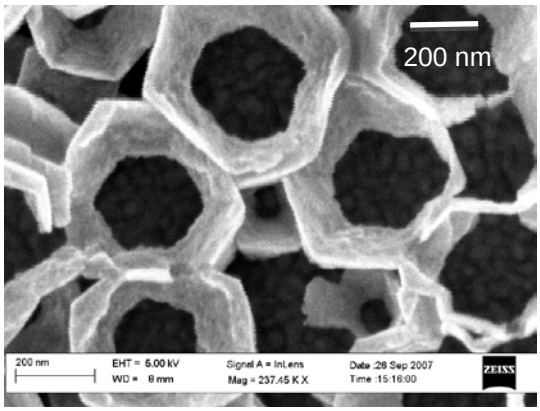

Figure 7. Formation of ultra-thin-walled tubes. The applied potential was -970 mV (vs. Ag/AgCl), using a 5 mM $Zn(NO_3)_2$ solution and 0.1 M $CaCl_2$ electrolyte.

CONCLUSIONS

The selective dissolution of electrodeposited ZnO nanorods has been explained in terms of the anisotropy of the ZnO surface energy. The dissolution process is controlled by the surface stability of the rods in solution and the diffusion of reactants. The rod diameter and chloride stabilization of the (002) plans play a critical role in determining the nanostructure morphology. Homogenous dissolution or selective etching of the (110) and (002) surfaces can be controlled. The formation of rods with a thin diameter, cavity or tubular structures can be achieved by anisotropic dissolution. The dimensionality (e.g. aspect ratio and wall thickness) of the structures can be controlled by an appropriate choice of the initial deposition and dissolution parameters.

AUTHOR INFORMATION

Corresponding Author

*To whom correspondence should be addressed. E-mail: iris@soton.ac.uk

Author Contributions

All authors have given approval to the final version of the manuscript.

Funding Sources

Funding was provided in part by the New Zealand Foundation for Research, Science and Technology under contract CO8X0409.

ACKNOWLEDGMENT

XAS data reported in this paper were collected at beamline X10C at the National Synchrotron Light Source. Use of the National Synchrotron Light Source, Brookhaven National Laboratory, was supported by the U.S. Department of Energy, Office of Basic Energy Sciences. The authors wish to thank Hugh Isaacs and Kenneth Sutter (Materials Science at BNL), and Larry Fareria and Mike Sansone (NSLS at BNL) for their technical support. XRD data were collected using beamline 11-3 at the Stanford Synchrotron Radiation Laboratory, a national user facility operated by Stanford University on behalf of the U.S. Department of Energy, Office of Basic Energy Sciences. This work was funded in part by the EPSRC (EP/J500161/1).

REFERENCES

(1) Wan, Q.; Li, Q. H.; Chen, Y. J.; Wang, T. H.; He, X. L.; Li, J. P.; Lin, C. L. Fabrication and ethanol sensing characteristics of ZnO nanowire gas sensor *Appl Phys Lett* **2004,** 84, 3654-3656.

(2) Keis, K. A 5% efficient photoelectrochemical solar cell based on nanostructured ZnO electrodes. *Sol Energ Mat Sol C* **2002,** 73, 51-58.

(3) Wang, Z. L.; Song, J. Piezoelectric nanogenerators based on zinc oxide nanowire arrays. *Science* **2006,** 312, 242-246.

(4) Peulon, S.; Lincot, D. Cathodic electrodeposition from aqueous solution of dense or open- structured zinc oxide films. *Adv. Mater.* **1996,** 8, 166-170.

(5) P. Yang, H. Y., S. Mao, R. Russo, J. Johnson, R. Saykally, N. Morris, J. Pham, R. He, H.-J. Choi. Controlled Growth of ZnO Nanowires **and** Their Optical Properties. *Adv. Funct. Mater.* **2002,** 12, 323-331.

(6) Illy B., Shollock B. A., MacManus-Driscoll J. L., Ryan M P Electrochemical growth of ZnO nano-plates**.** *Nanotech.* **2005,** 16, 320.

(7) Xu, L.; Chen, Q.; Xu, D. Hierarchical ZnO nanostructures obtained by electrodeposition. *J. Phys. Chem. C* **2007,** 111, 11560-11565.

(8). Li, F.; Ding, Y.; Gao, P.; Xin, X.; Wang, Z. L. Single- Crystal Hexagonal Disks and Rings of ZnO: Low- Temperature, Large- Scale Synthesis and Growth Mechanism. *Angew. Chem. In. Ed.* **2004,** 43, 5238-5242.

(9) Vayssieres, L.; Keis, K.; Hagfeldt, A.; Lindquist, S. E. Three-dimensional array of highly oriented crystalline ZnO microtubes. *Chem. Mater.* **2001,** 13, 4395-4398.

(10) Luo, L.; Lv, G.; Li, B.; Hu, X.; Jin, L.; Wang, J.; Tang, Y. Formation of aligned ZnO nanotube arrays by chemical etching and coupling with CdSe for photovoltaic application. *Thin Solid Films* **2010,** 518, 5146-5152.

(11) Wu, X.-J.; Zhu, F.; Mu, C.; Liang, Y.; Xu, L.; Chen, Q.; Chen, R.; Xu, D. One-dimensional ZnO nanostructured films: Effect of oxide nanoparticles. *Coord. Chem. Rev.* **2010,** 254, 1135-1150.

(12) Wang, X.; Song, J.; Wang, Z. L. Nanowire and nanobelt arrays of zinc oxide from synthesis to properties and to novel devices. *J. Mater. Chem* **2007,** 17, 711-720.

(13) Sun, Y.; Fuge, G. M.; Fox, N. A.; Riley, D. J.; Ashfold, M. N. R. Synthesis of aligned arrays of ultrathin ZnO nanotubes on a Si wafer coated with a thin ZnO film. *Adv. Mat.* **2005,** 17, 2477-2481.

(14) Kong, X.; Sun, X.; Li, X.; Li, Y. Catalytic growth of ZnO nanotubes. *Mat.Chem. Phys.* **2003,** 82, 997-1001.

(15) Yu, H.; Zhang, Z.; Han, M.; Hao, X.; Zhu, F. A general low-temperature route for large-scale fabrication of highly oriented ZnO nanorod/nanotube arrays. *J. Am. Chem. Soc.* **2005,** 127, 2378-2379.

(16) Sun, Y.; George Ndifor-Angwafor, N.; Jason Riley, D.; Ashfold, M. N. R. Synthesis and photoluminescence of ultra-thin ZnO nanowire/nanotube arrays formed by hydrothermal growth. *Chem. Phys. Lett.* **2006,** 431, 352-357.

(17) Ren, X.; Jiang, C. *J.* Synthesis of ZnO Nanotube Arrays and Heterostructures of Cu–ZnO Coaxial Nanotubes by Electrodeposition–Oxidation Method *J. Nanosci. Nanotechnol.* **2010,** 10, 5093-5098.

(18) Yang, J.; Liu, G.; Lu, J.; Qiu, Y.; Yanga, S. Electrochemical route to the synthesis of ultrathin ZnO nanorod/nanobelt arrays on zinc substrate. *Appl. Phys. Lett.* **2007,** 90, 103109.

(19) Yu, L.; Zhang, G.; Li, S.; Xi, Z.; Guo, D. Fabrication of arrays of zinc oxide nanorods and nanotubes in aqueous solution under an external voltage. *J. Cryst. Growth* **2007,** 299, 184-188.

(20) Tang, Y.; Luo, L.; Chen, Z.; Jiang, Y.; Li, B.; Jia, Z.; Xu, L. Electrodeposition of ZnO nanotube arrays on TCO glass substrates. *Electrochem. Comm.* **2007,** 9, 289-292.

(21) Q.; Zhang, J.; Ai, X.; Xu, D. *J Phys Chem. C* **2007,** 111, 4549-4552.

(22) Han, J. ZnO nanotube-based dye-sensitized solar cell and its application in self-powered devices. *Nanotechnology* **2010,** 21, 405203.

(23) Gan, X.; Li, X.; Gao, X.; Yu, W. Investigation on chemical etching process of ZnO nanorods toward nanotubes. *J. Alloy Comp.* **2009,** 481, 397-401.

(24) Su, J.; Che, R. C.; She, G. W.; Duan, X. F.; Shi, W. S. Transmission Electron Microscopy of ZnO Nanotube Arrays Etched from Electrodeposited ZnO Nanorods. *J. Nanosci. Nanotechnol.* **2008,** 8, 6306-6309.

(25) Yu, Q.; Fu, W.; Yu, C.; Yang, H.; Wei, R.; Li, M.; Liu, S.; Sui, Y.; Liu, Z.; Yuan, M.; Zou, G.; Wang, G.; Shao, C.; Liu, Y. Fabrication and Optical Properties of Large-Scale ZnO Nanotube Bundles via a Simple Solution Route. *J. Phys Chem. C* **2007,** 111, 17521-17526.

(26) She, G.; Zhang, X.; Shi, W.; Fan, X.; Chang, J. C. Electrochemical/chemical synthesis of highly-oriented single-crystal ZnO nanotube arrays on transparent conductive substrates. *Electrochem Comm.* **2007,** 9, 2784-2788.

(27) Elias, J.; Tena-Zaera, R.; Wang, G.-Y.; Levy-Clement, C. Conversion of ZnO Nanowires into Nanotubes with Tailored Dimensions. *Chem. Mat.* **2008,** 20, 6633-6637.

(28) She, G. W.; Zhang, X. H.; Shi, W. S.; Fan, X.; Chang, J. C.; Lee, C. S.; Lee, S. T.; Liu, C. H. Controlled synthesis of oriented single-crystal ZnO nanotube arrays on transparent conductive substrates. *Appl. Phy. Lett.* **2008,** 92, 5

(29) Yan, C.; Xue, D. Electroless deposition of aligned ZnO taper-tubes in a strong acidic medium. *Electrochem. Comm.* **2007,** 9, 1247-1251.

(30) Illy, B. N.; Ingham, B.; Ryan, M. P. Effect of supersaturation on the growth of zinc oxide nanostructured films by electrochemical deposition. *Cryst. Growth Des.* **2010,** 10, 1189-1193.

(31) Goux, A.; Pauporte, T.; Chivot, J.; Lincot, D. Temperature effects on ZnO electrodeposition. *Electrochim. Acta* **2005,** 50, 2239-2248.

(32) Atienzar, P.; Ishwara, T.; Illy, B. N.; Ryan, M. P.; O'Regan, B. C.; Durrant, J. R.; Nelson, J. Control of Photocurrent Generation in Polymer/ZnO Nanorod Solar Cells by Using a Solution-Processed TiO_2 Overlayer. *J. Phys. Chem. Lett.* **2010,** 1, 708-713.

(33) Schumann, S.; Da Campo, R.; Illy, B.; Cruickshank, A. C.; McLachlan, M. A.; Ryan, M. P.; Riley, D. J.; McComb, D. W.; Jones, T. S. Inverted organic photovoltaic devices with high efficiency and stability based on metal oxide charge extraction layers. *J. Ma.t Chem.* **2010**, 21, 2381-2386.

(34) Wong, M.; Berenov, A.; Qi, X.; Kappers, M.; Barber, Z.; Illy, B., Lockman, Z, Ryan, M P, MacManus-Driscoll, J L. Electrochemical growth of ZnO nano-rods on polycrystalline Zn foil. *Nanotechnology* **2003,** 14, 968-973.

(35) Ingham, B.; Illy, B. N.; Ryan, M. P. In situ synchrotron studies of ZnO nanostructures during electrochemical deposition. *Cur. Appl. Phys.* **2008,** 8, 455-458.

(36) Ingham, B.; Illy, B. N.; Ryan, M. P. Direct observation of distinct nucleation and growth processes in electrochemically deposited ZnO nanostructures using in situ XANES. *J. Phys. Chem. C* **2008,** 112, 2820-2824.

(37) Ingham, B.; Illy, B. N.; Toney, M. F.; Howdyshell, M. L.; Ryan, M. P. In Situ Synchrotron X-ray Diffraction Experiments on Electrochemically Deposited ZnO Nanostructures. *J. Phys. Chem. C* **2008,** 112, 14863-14866.

(38) Illy, B. N.; Cruickshank, A. C.; Schumann, S.; Da Campo, R.; Jones, T. S.; Heutz, S.; McLachlan, M. A.; McComb, D. W.; Riley, D. J.; Ryan, M. P. Electrodeposition of ZnO layers for photovoltaic applications: controlling film thickness and orientation. *J. Mat. Chem.***2011**, 21, 12949-12957.

(39) Wander, A.; Harrison, N. M. An ab-initio study of ZnO (1120). *Surf. Sci.* **2000,** 468, L851-L855.

(40) Tena-Zaera, R.; Elias, J.; Wang, G.; Levy-Clement, C. Role of Chloride Ions on Electrochemical Deposition of ZnO Nanowire Arrays from O_2 Reduction. *J. Phy.s Chem. C* **2007,** 111, 16706-16711.

(41) Dulub, O., Diebold, U and Kresse, G.; . Novel Stabilization Mechanism on Polar Surfaces: ZnO(0001)-Zn. *Phys. Rev. Lett.* **2003,** 90, 016102-1-016102-4.

(42) Pedersen, T. G., Quantum size effects in ZnO nanowires. *Phys Stat. Sol. C* **2005,** 2, 4026-4030.

SYNOPSIS TOC: Zinc oxide nanorods can be selectively etch to form nanorods with a smaller diameter, nanotubes or cavities with controllable dimensions. We explained the underlying parameters controlling the dissolution behavior for the first by rationalizing it in terms of surface energy and diffusion of the reactant.

Table of Contents artwork here